

## Interannual Variability in the Mid- and Low-Latitude Western North Pacific\*

BO QIU AND TERRENCE M. JOYCE

*Department of Physical Oceanography, Woods Hole Oceanographic Institution, Woods Hole, Massachusetts*

(Manuscript received 17 June 1991, in final form 20 November 1991)

### ABSTRACT

Twenty-two years (1967–88) of hydrographic data collected by the Japan Meteorological Agency along the 137°E meridian and surface wind data compiled by Florida State University (FSU) were analyzed to study the interannual variability in the western North Pacific.

In the midlatitude region north of 22°N, the dominant signal in the dynamic height field was the interannual path variations of the Kuroshio. Whereas the eastward transport of the Kuroshio itself had no significant changes between the straight-path and meander-path years, the net transport of the Kuroshio system including recirculations showed a 30% increase during the meander-path years. In the straight-path years when the net transport was small, the Kuroshio tended to take a straight path with a strong recirculation developed to the south. The interannual path variations of the Kuroshio strongly influenced the water-mass movement in the midlatitudes. During the Kuroshio meander years, we found that a significant portion of the North Pacific Intermediate Water east of the Kuroshio meander was blocked from subducting farther westward. In the middepth layer of 1500–2500 m, analysis of the  $\theta$ - $S$  relation revealed a water-mass movement negatively correlated to the upper-layer Kuroshio path changes, implying a possible compensating flow in the middepth layer for the cold-core eddy emerging north of the Kuroshio.

In the low-latitude region along 137°E, fluctuations in the surface height anomaly field had a meridionally coherent structure, and large surface height drops coincided with the ENSO events in the tropical Pacific. Accompanying the surface height drops in the ENSO years was an increase in the transport of both the North Equatorial Current (NEC) and the North Equatorial Countercurrent (NECC) and a southward shift in the boundary of the NEC and NECC. Based on the FSU surface wind data, we found that these interannual fluctuations of the NEC and the NECC were highly correlated to the Sverdrup transport fluctuations estimated from the basinwide wind-stress curl field. Using a reduced-gravity model and simplified patterns of wind forcing, we showed that this high correlation came about because the center of the interannual signal of the wind-stress curl field is close to the western Pacific (near the date line) and because the thermocline tilt in the NEC region attenuates the strong latitude dependence of the phase speed of the long baroclinic Rossby wave.

### 1. Introduction

Interannual variations in sea level and surface dynamic height of the North Pacific have long been recognized as accounting for a significant portion of the total variability. Using sea level observations from the central North Pacific, Wyrski (1974) found that the surface flows in both the North Equatorial Current (NEC) and the North Equatorial Countercurrent (NECC) fluctuated  $\pm 25\%$  from their respective means in the interannual frequency band. In the midlatitude North Pacific, analyses of historical hydrographic and bathythermograph data by White (1975, 1977) also showed that the interannual changes in the dynamic height varied about 25% from the mean values.

In the North Pacific west of 140°E, the midlatitude interannual signal is largely represented by the bimodal path variations of the Kuroshio: A straight path denotes the Kuroshio flowing along the Japan coast, whereas a meander path denotes that it is taking a stable southward detour (e.g., Shoji 1972; Taft 1972). One of the crucial factors in determining the path bimodality is thought to be the interannual fluctuation of the Kuroshio transport. Whether or not the Kuroshio transport decreases during the meander period has been a subject of debate over the past decade. Based on hydrographic surveys from 1955 to 1968, Nitani (1972) found that the geostrophic transport of the Kuroshio south of Japan (along 135.5°E with a reference level at 1000 db) decreased during the meander period of 1959–63. His result had a profound impact upon later theoretical and numerical studies aiming to explain the interannual variations of the Kuroshio path. Studies by White and McCreary (1976), Masuda (1982), Chao and McCreary (1982), and Yasuda et al. (1985) have all shown that the Kuroshio takes a meander (straight) path when the upstream transport of the Kuroshio is

\* Woods Hole Oceanographic Institution Contribution Number 7829.

Corresponding author address: Dr. Bo Qiu, Dept. of Physical Oceanography, Woods Hole Oceanographic Institution, Woods Hole, MA 02543.

small (large). On the other hand, analyses of the Kuroshio transport at the upstream region in the East China Sea (using hydrographic data by Saiki 1982) and across the Tokara Strait (using sea level data by Kawabe 1980) showed that the Kuroshio transport is larger in the meander-path years than in the straight-path years. By including a more realistic inclination of the Japan coast relative to the due east in numerical calculations, several recent studies have shown that a larger upstream transport is more likely to induce the Kuroshio meander (Chao 1984; Yoon and Yasuda 1987; Akitomo et al. 1991).

With the reoccurrence of meander events in 1982–84 and 1987–88, it is now possible to reexamine the relationship between the interannual variations of the Kuroshio transport and its path changes. Another point addressed in this study is how the Kuroshio path variations are related to fluctuations of subsurface water masses such as the North Pacific Intermediate Water (Reid 1965; Masuzawa 1972), and of the water-mass movement below the thermocline. Clarifying these relations not only is important to our understanding of these water masses, but also sheds light on causes of the Kuroshio path bimodality.

In the low-latitude North Pacific, many authors have studied interannual fluctuations in sea level and dynamic height and their connections with the El Niño–Southern Oscillation (ENSO) events of the tropical Pacific (Wyrski 1975, 1979; Masuzawa and Nagasaka 1975; White and Hasunuma 1980; Meyers 1982; White et al. 1985a,b; Kessler and Taft 1987). For the western North Pacific in particular, White and Hasunuma (1980) showed that the NEC and the Kuroshio Countercurrent fluctuated in phase, whereas their fluctuations were out of phase with those of the NECC. Within the data period of 1954–74, they found the NEC tended to weaken during ENSO events. In contrast, Wyrski (1979) showed that in the central Pacific the NEC and the NECC fluctuated in phase and their transports were large during ENSO periods.

Most studies on the interannual fluctuations of the western North Pacific have been based on tidal station data or dynamic height data from ship observations averaged in a  $2.5^\circ$  latitude by  $5^\circ$  longitude box. Their ability to resolve velocity profiles and transports of the ocean currents was thus rather poor, especially considering that some of the major currents in this region have a width of only a few degrees and that they may migrate considerably in the meridional direction. Initiated as part of the Cooperative Study of the Kuroshio (CSK) to monitor the ocean circulation in the western North Pacific, hydrographic surveys have been conducted by the Japan Meteorological Agency along the  $137^\circ\text{E}$  meridian every winter since 1967 and every summer since 1972 (Masuzawa and Nagasaka 1975; Andow 1987). Accumulation of these repeated surveys provided us a new opportunity to look into the interannual fluctuations in the low- and midlatitude western North Pacific.

Based on these hydrographic surveys, this paper first describes the mean structures along the  $137^\circ\text{E}$  meridian together with a brief comparison with the rest of the North Pacific (section 3). In section 4, interannual fluctuations in the Kuroshio and the Kuroshio Countercurrent, as well as their relation to Kuroshio path changes, are investigated. Also investigated in this section is the relation between the Kuroshio path changes and water-mass variations at a depth of 1000–2500 m. Section 5 focuses on the interannual fluctuations in low latitudes: transports of the NEC and the NECC, anomalies in the surface height and upper-layer thickness fields, and their connections to the ENSO events. Since the interannual fluctuations in the low latitudes are plausibly caused by changes in the wind-stress curl at the sea surface (Wyrski 1975; Wyrski and Meyers 1976), the FSU wind data are analyzed in section 6. A simple model is used to further clarify connections between the interannual fluctuations in the western North Pacific and in the basinwide wind-stress curl field. Conclusions are summarized in section 7.

## 2. Data

### a. Hydrographic data

The biannual hydrographic surveys by the Japan Meteorological Agency are along  $137^\circ\text{E}$  near the western periphery of the tropical and subtropical gyres of the North Pacific (Fig. 1). The hydrographic section crosses from the coast of Japan ( $34^\circ\text{N}$ ) to New Guinea ( $1^\circ\text{S}$ ). Stations along the hydrographic section are located approximately  $0.5^\circ$  apart in the tropical region ( $1^\circ\text{S}$ – $8^\circ\text{N}$ ) and  $1^\circ$  apart for the remaining northern region. Nominal vertical sampling is 20–50 m for the surface–250-m layer and 100–200 m to a depth of 1000–1500 m. Deeper observations, extending to a depth of 4000 m, were also performed but had a poorer resolution in both vertical (500–1000 m) and horizontal ( $5^\circ$ ) directions. For most of the winter cruises, the RV *Ryofu-Maru* also carried out detailed surveys of the Kuroshio south of Japan. Hydrographic data in the vicinity of  $137^\circ\text{E}$  from these supplementary measurements were also used in our study.

Hydrographic data from 22 winter cruises (1967–88) and 17 summer cruises (1972–88) were used in this study. To remove spurious outliers in the data, we first grouped the observational stations into seven bins, each of which had a  $5^\circ$  width and was centered at  $2^\circ\text{N}$  to  $32^\circ\text{N}$ . In each bin, a mean curve of the potential temperature versus the salinity ( $\theta$ – $S$ ) was determined using the cubic spline fit (Armi and Bray 1982) and standard deviation values from this mean curve were then calculated. Data outside the two-standard-deviation boundaries were automatically rejected, whereas those falling between the one- and the two-standard-deviation boundaries were discarded subjectively only when the datum was isolated on the  $\theta$ – $S$  diagram. About 0.5% of the data were eliminated according to

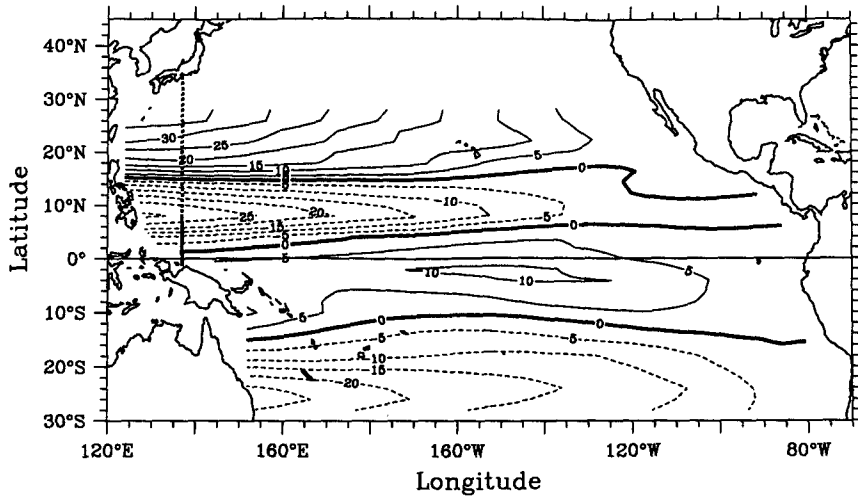


FIG. 1. Sverdrup transports in the Pacific Ocean based on the FSU surface wind data averaged from 1961 to 1987. Units are  $10^6 \text{ m}^3 \text{ s}^{-1}$  ( $=\text{Sv}$ ). The dots along the  $137^\circ\text{E}$  meridian denote the hydrographic stations by the RV *Ryofu-Maru* of the Japan Meteorological Agency.

these rejection criteria. Figure 2 shows the mean  $\theta$ - $S$  curves in the seven bins recalculated after removing the questionable data.

After quality control, the irregularly spaced station data in the meridional section were interpolated and smoothed onto a common grid. The grid had a horizontal resolution of  $0.5^\circ$  for the upper 1500-m layer and  $1^\circ$  for the layer below. Vertical resolution was 25 m for the surface-250-m layer, 50 m for the layer between 250 and 1500 m, and 250 m for the layer below 1500 m. Spacings in both directions were essentially determined by available observations. To estimate  $\theta$  and  $S$  values on the grid point, the observational data were first linearly interpolated in depth and then smoothed horizontally using the objective analysis scheme described by Levitus (1982). The influence radii used in the objective analysis were  $1.5^\circ$  latitude for the upper 1500-m layer and  $5^\circ$  latitude for the layer below.

#### b. Wind data

Monthly wind-stress data over the entire Pacific Ocean between  $30^\circ\text{S}$  and  $30^\circ\text{N}$  have been produced by the Mesoscale Air-Sea Interaction Group at Florida State University (FSU) based on ship winds subjectively analyzed onto a  $2^\circ$  latitude by  $2^\circ$  longitude grid (Goldenberg and O'Brien 1981). This wind dataset was used in the present study to elucidate possible relations between the atmospheric forcing and the inter-annual variability observed in the western North Pacific. The pseudostress values of the FSU wind data were converted to stress using a value of  $1.5 \times 10^{-3}$  for the drag coefficient and the wind-stress curl was calculated using central differencing. The Sverdrup transport based on the FSU wind-stress data averaged from 1961 through 1987 is shown in Fig. 1. The trans-

port pattern resembles that estimated by Kessler and Taft (1987, their Fig. 26), who used a 3-year (1979-81) average of the FSU wind-stress data.

### 3. Mean structures along the $137^\circ\text{E}$ meridian

As a basis for understanding the variability along the  $137^\circ\text{E}$  meridian, we will start with the mean oceanic

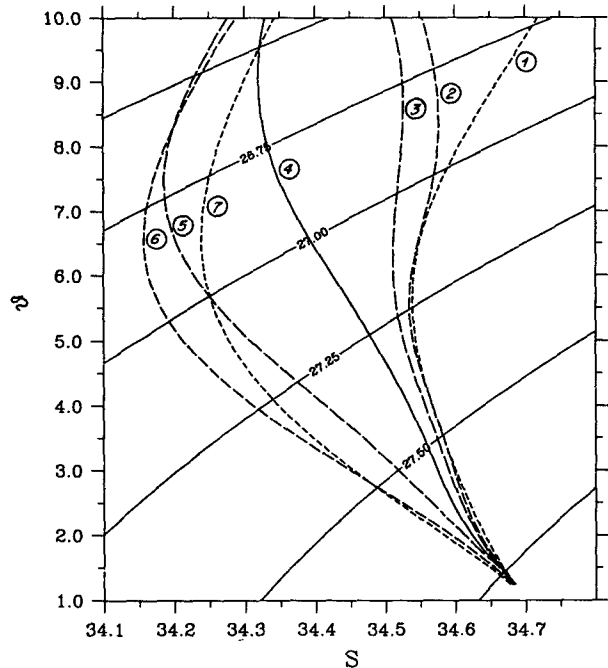


FIG. 2.  $\theta$ - $S$  relations averaged in the seven  $5^\circ$  width bins along the  $137^\circ\text{E}$  meridian. The center latitude for each bin is  $5^\circ \times n - 3^\circ$ , where  $n$  is the bin number and is denoted next to the corresponding  $\theta$ - $S$  curve in the figure.

features along this meridian and briefly discuss their relationship to the rest of the western North Pacific. The main thermocline along 137°E is most intense between 5°N and 10°N with the isotherms spreading progressively apart to the north and south (Fig. 3a). The ridge of the thermocline, situated at 7.5°N in this region, forms the boundary between the North Equatorial Current and the North Equatorial Countercurrent. Based on the distributions of the 20°C isotherm depth, Kessler (1990) has shown that the mean position of this thermocline ridge is nearly zonal (between 7.5°N and 10°N) across the entire North Pacific. In regions of 20°–30°N between the seasonal and the main thermoclines (170 and 400 m), a water mass with a minimum in the vertical potential density gradient exists. This water mass, known as the Subtropical Mode Water (Masuzawa 1969, 1972), forms in the northern edge of the subtropical gyre through wintertime convective mixed-layer processes and is believed to be advected to the western Pacific by the westward-flowing Kuroshio Countercurrent (Hanawa 1987; Suga et al. 1989). In Fig. 3a, the thermocline rises sharply near the coast of Japan, corresponding to the western boundary current, the Kuroshio.

In the equatorial region along the 137°E meridian, the isotherms are essentially horizontal, indicating that no equatorial undercurrent, as a time average, exists at this western portion of the equatorial Pacific. This feature, also noted by Toole et al. (1988) using historical temperature and salinity data, is different from the meridional distributions of the mean water temperature observed in the central equatorial Pacific, where the isotherms at the 200-m depth bulge vertically in connection with the Equatorial Undercurrent (EUC) (e.g., Wyrтки and Kilonsky 1984; Lukas and Firing 1984). A recent observational study by Tsuchiya et al. (1989) indicated that a major portion of the New Guinea coastal undercurrent (centered at the 200 m depth) reaches the equator north of Papua New Guinea and deflects to the east to feed the EUC. Absence of the EUC in Fig. 3a suggests that the eastward deflection of the New Guinea coastal undercurrent largely occurs east of the 137°E meridian.

The salinity structures along the 137°E meridian are characterized by the existence of three extrema and a broad uniform salinity region in the midlayer low latitude (Fig. 3b). The salinity maximum near the equator has a core (with a salinity maximum > 35.4 psu) along the New Guinea coast at a depth of 150 m. This maximum salinity water is possibly influenced by the New Guinea coastal undercurrent, which transports high-salinity, high-oxygen water from the Solomon Sea into the western equatorial Pacific (Tsuchiya et al. 1989). A second salinity maximum has a core around 15°N at a depth of 150 m (maximum salinity > 35.0 psu). This salinity maximum also appears in the mean salinity distribution across the central Pacific (around 160°W; Reid 1965; Robinson 1976; Wyrтки and Kilonsky 1984) and it is caused by excess of evaporation

over precipitation and by long residence of the surface water in the central Pacific (see Masuzawa 1972).

A prominent salinity minimum region can be seen in Fig. 3b to extend through the subtropical gyre from the NEC to the Kuroshio (see Fig. 4). It has a core at 24°N and 750-m depth and lies on the 26.8 $\sigma_\theta$  (125  $\text{cl t}^{-1}$ ) isopycnal surface along the 137°E meridian (Fig. 3c). This salinity minimum water is commonly known as the North Pacific Intermediate Water (NPIW) and is shown by Reid (1965) to exist over most of the mid-latitude North Pacific on the 26.8 $\sigma_\theta$  isopycnal surface. Reid speculated that the NPIW is formed in the sub-arctic region, where vertical mixing and atmospheric cooling cause low-salinity surface water to deepen and be transmitted southwestward through lateral mixing and advection. Recently, Talley (1991) suggested that the low-salinity water mass of the NPIW may have its origin in the Okhotsk Sea.

From the temperature and salinity distributions shown in Fig. 3, mean zonal geostrophic flow relative to 1000 db was computed (Fig. 4). Due to small values of the Coriolis parameter, geostrophic flows near the equator indicated large and unrealistically swift fluctuations, and were consequently excluded from the present study. This exclusion prevented us from estimating the transports of the South Equatorial Current and the New Guinea coastal undercurrent, but it had negligible influence on the NECC that has its main body north of 2°N. The mean transport values of the NECC (eastward flow from 2°N to 7°N) and the NEC (westward flow from 7°N to 25°N) in Fig. 4 are 42.1 Sv and -59.4 Sv, respectively. In evaluating the transport for the NECC, many former studies have defined it as the eastward flow above a particular isotherm/isopycnal: for example, the 14°C isotherm by Wyrтки and Kilonsky (1984), the 12°C isotherm by Toole et al. (1988), and the 23.5 $\sigma_\theta$  isopycnal by Delcroix et al. (1987). Eastward flow below such an isotherm/isopycnal is known as the Northern Subsurface Countercurrent (Tsuchiya 1975). Along the 137°E meridian, the transport of the mean NECC reduces to 28.0 Sv ( $\text{Sv} \equiv 10^6 \text{ m}^3 \text{ s}^{-1}$ ) if the 12°C isotherm, which lies at the base of the thermocline, is chosen.

The mean geostrophic transport across 137°E can be compared to the mean Sverdrup transport divergence by integrating the Sverdrup balance zonally from the eastern boundary and examining meridional differences. In the NEC region of 7°–25°N, the geostrophic transport (-59.4 Sv) is close to that from the Sverdrup balance (-63 Sv, Fig. 1). While the transport of the NECC from the geostrophic calculation (42.1 Sv) is about 50% larger than that estimated from the Sverdrup relation (about 28 Sv), this Sverdrup transport value agrees with the geostrophic transport value if the NECC is defined as an eastward flow above the 12°C isotherm. This difference will be further discussed in section 6.

Within the zonal band of 20°–28°N, individual geostrophic flow profiles indicated weak currents, with

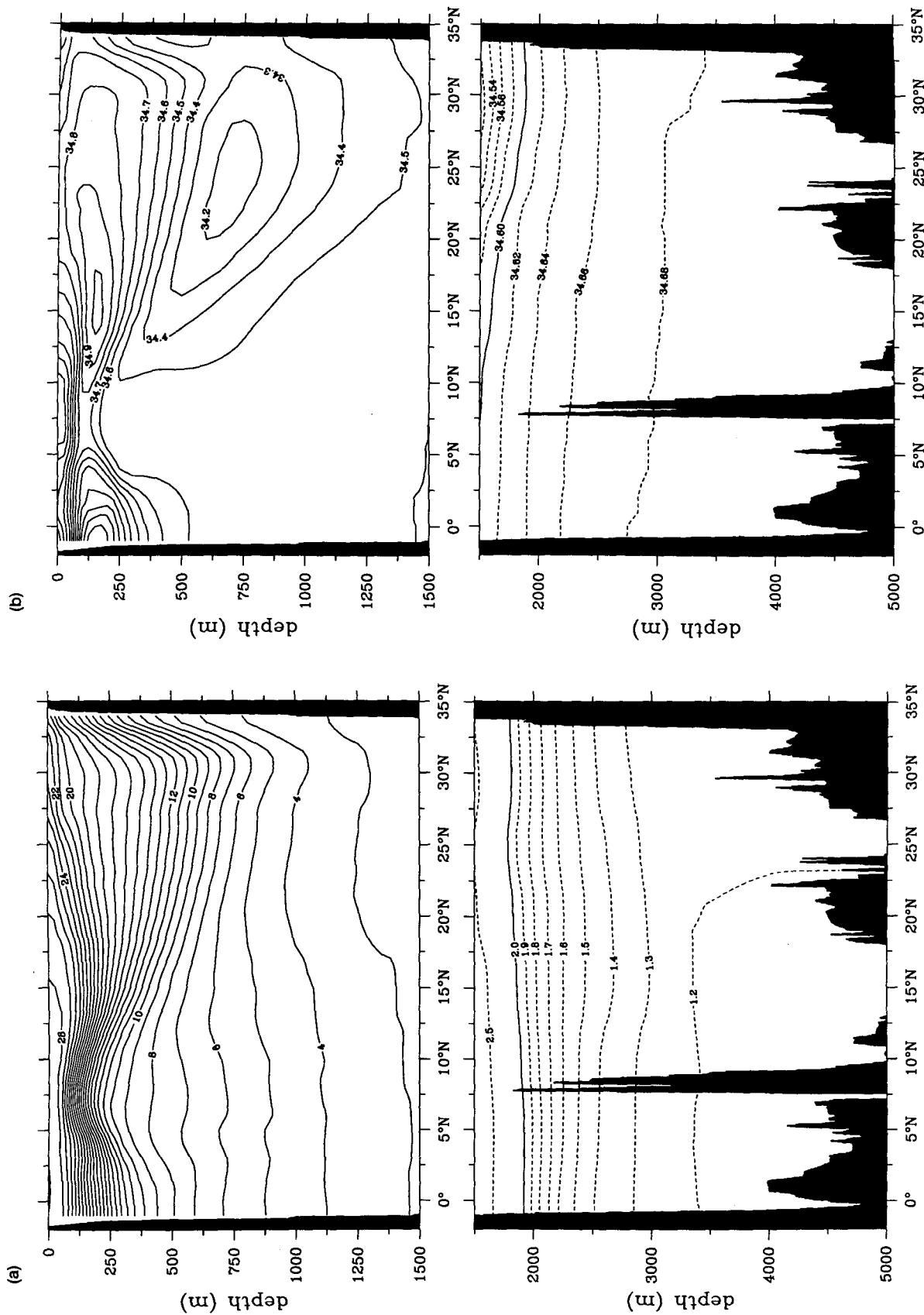


FIG. 3. Meridional distributions of (a) potential temperature in °C, (b) salinity in practical salinity units (psu), (c)  $\sigma_t$  along the 137°E meridian. Values are averaged over the 39 cruises from 1967 to 1988.

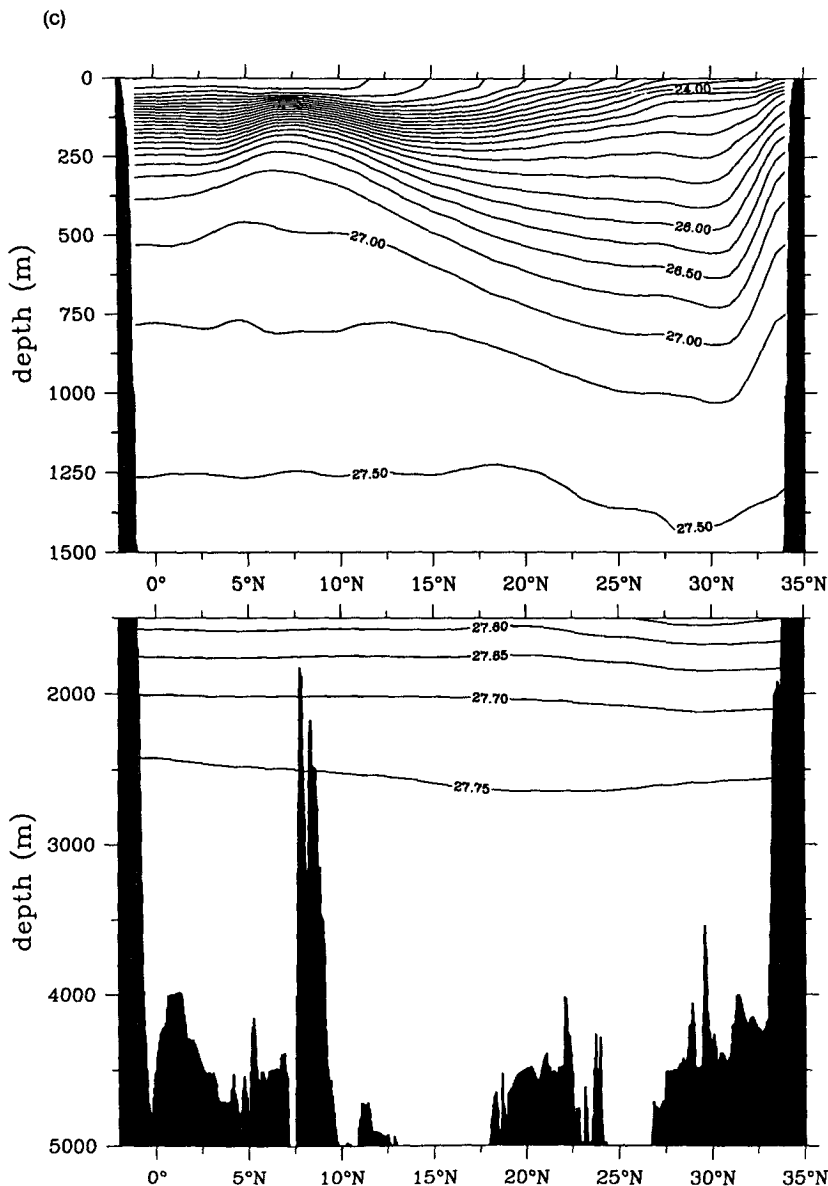


FIG. 3. (continued)

a magnitude of a few centimeters per second, flowing alternately to the east and west (not shown). A semi-permanent eastward flow exists in this region and is sometimes called the subtropical countercurrent (Yoshida and Kidokoro 1967). Its existence, however, is only barely discernible in the mean flow pattern of Fig. 4. A more systematic westward flow, the Kuroshio Countercurrent (KCC), exists between 27.5° and 29.5°N and is a recirculating portion of the Kuroshio south of Japan. The transport values for the mean Kuroshio and KCC in Fig. 4 are 36.1 Sv and -3.7 Sv, respectively. Due to extensive lateral excursions of the Kuroshio, these transport values, estimated from geographically fixed regions, are much smaller than those

established by previous studies. Notice that the total mean transport of the Kuroshio and the KCC remains approximately the same whether it is estimated from a geographically fixed coordinate (32.4 Sv from Fig. 4) or a stream coordinate (33.0 Sv, see section 4). Not surprisingly, this transport is close to the Sverdrup inflow of the subtropic gyre (~36 Sv from Fig. 1).

**4. Midlatitude interannual variability**

To investigate the interannual variability in the western North Pacific, we first computed the surface dynamic height for the 39 cruises and constructed the mean surface dynamic height profiles for the winter

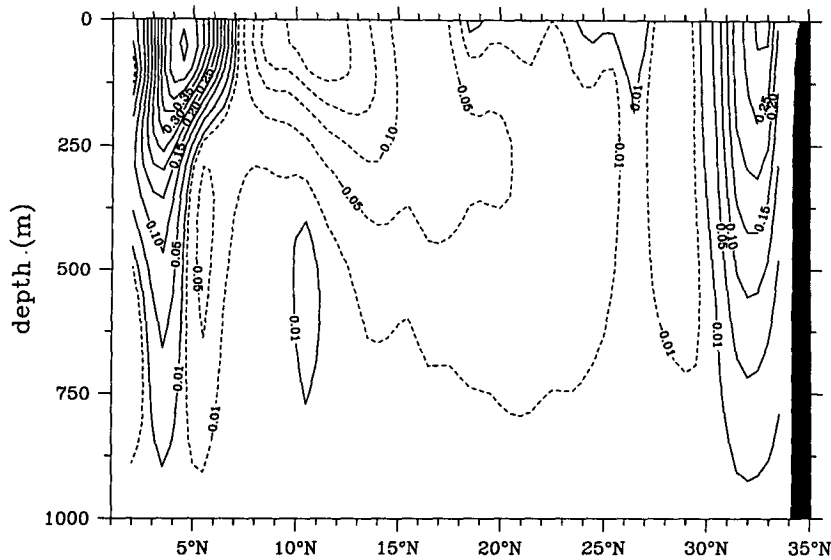


FIG. 4. Mean zonal geostrophic flows relative to 1000 db along the 137°E meridian (averaged from 1967 to 1988). Solid contours indicate eastward flows, and dashed contours westward flows. Units are meters per second.

and summer seasons. Height anomalies were then calculated by subtracting the seasonal mean profile from the individual cruise profiles. Figure 5 shows the height anomaly fluctuations as a function of time and latitude. Since the time scales of the height anomalies in the mid- and low latitudes are different, we will first focus on the midlatitude fluctuations.

In the midlatitudes north of 25°N, the dominant interannual signals in Fig. 5 appear in the Kuroshio region offshore of Japan. While large in amplitude, the

fluctuations are aperiodic and the duration of the individual height anomalies varies from a period of 1 year to 5 or 6 years. Using hydrographic observations, Kawai (1969) showed that the Kuroshio axis south of Japan can be adequately represented by the 15°C isotherm at a 200-m depth. Based on this criterion as well as quarterly data reports from the Japan Meteorological Agency and Japan Oceanographic Data Center, we plot in Fig. 6 the time series of the Kuroshio axis position along the 137°E meridian. Comparison of Figs. 5 and

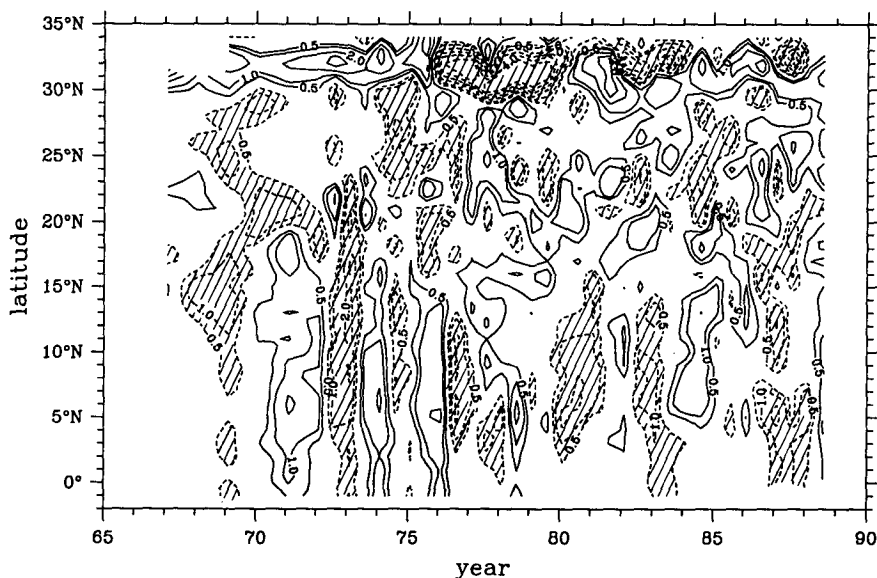


FIG. 5. Surface dynamic height anomalies (0/1000 db) calculated from individual cruise data. Notice that seasonal means have been removed from this anomaly field. Shaded regions indicate negative anomalies. Units:  $\text{m}^2 \text{s}^{-2}$ .

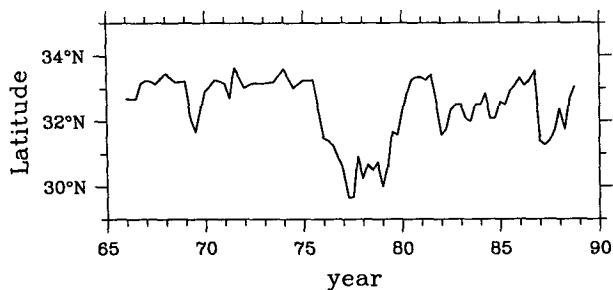


FIG. 6. Latitudinal position of the Kuroshio axis (the 15°C isotherm at the 200-m depth) along the 137°E. Water temperature data are based on data reports of Japan Meteorological Agency and Japan Oceanographic Data Center.

6 clearly shows that the negative anomalies in the surface height field correspond to the meander-path years of the Kuroshio. The Kuroshio meander was particularly prominent during the years 1976–80, and several studies have given detailed descriptions of the evolution of this meander and the accompanying large cold-core eddy between it and the Japan coast (Kawabe 1980, 1985; Sekine and Toba 1981; Nishida 1982; Ishii 1982).

Based on the temperature and salinity observations, we calculated the geostrophic transports of the Kuroshio, the Kuroshio Countercurrent, and the westward flow associated with the large cold-core eddy north of the Kuroshio. The Kuroshio transport is defined as the total eastward flow north of 30°N and the KCC is the westward flow south of the Kuroshio. The reference level was chosen at 1250 m, the deepest common level of closely spaced observations. Since both the KCC and the westward flow of the cold-core eddy, which develops when the Kuroshio takes a meander path, can be regarded as recirculating components of the Kuroshio, the sum of these three flows is hereafter interpreted as the net transport of the Kuroshio across the 137°E meridian.

Figure 7 shows the time series of the Kuroshio transport (dashed line) and the net transport of the Kuroshio (solid line). The mean transport value of the Kuroshio, 52.4 Sv (Table 1), is similar to that found by Nitani

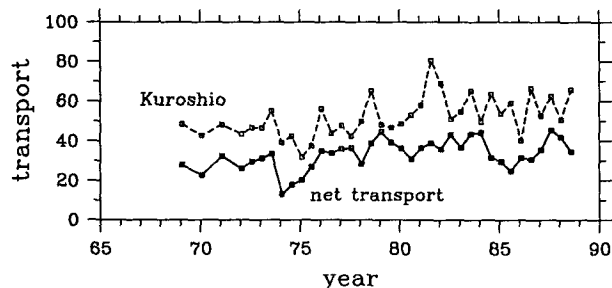


FIG. 7. Time series of the Kuroshio transport (dashed line) and the net transport of the Kuroshio, namely, the total transport of the Kuroshio, the Kuroshio Countercurrent, and the westward flow associated with the cold-core water mass between the meandering Kuroshio and the Japan coast (solid line). Units: Sv.

TABLE 1. Geostrophic transport of the Kuroshio, the Kuroshio Countercurrent, the net Kuroshio (transport), the North Equatorial Current, and the North Equatorial Countercurrent averaged over different years. Units are  $10^6 \text{ m}^3 \text{ s}^{-1}$  ( $\equiv \text{Sv}$ ) (see Table 2 for transport values from individual cruises).

|                     | Kuroshio | KCC   | net Kuroshio | NEC   | NECC |
|---------------------|----------|-------|--------------|-------|------|
| Total mean          | 52.4     | -18.1 | 33.0         | -62.3 | 51.5 |
| Winter mean         | 49.7     | -16.2 | 32.1         | -58.5 | 48.9 |
| Summer mean         | 55.7     | -20.5 | 34.0         | -67.2 | 54.9 |
| Straight-path years | 52.5     | -23.4 | 28.9         | —     | —    |
| Meander-path years  | 52.2     | -10.9 | 38.6         | —     | —    |
| ENSO years          | 52.5     | -17.0 | 35.3         | -70.8 | 68.6 |
| Non-ENSO years      | 52.3     | -18.8 | 31.8         | -57.0 | 42.3 |

(1975), who estimated the mean geostrophic transport of the Kuroshio (1947–73) across the longitudes of 137°–138°40'E to be  $\sim 55 \text{ Sv}$ . Inconsistent with Nitani's result, the time series shown in Fig. 7 shows no apparent difference in the transport values between the Kuroshio straight-path and meander-path years. Averaging the transport values over the straight-path and meander-path years revealed that the mean transport values in these two periods are not statistically different (Table 1). This, however, is not the case for the net transport of the Kuroshio, which depends significantly on the intensity of the KCC. During the meander-path years, the KCC tends to diminish substantially: its transport averaged in the meander-path years ( $-10.9 \text{ Sv}$ , Table 1) is less than half that in the straight-path years ( $-23.4 \text{ Sv}$ ). As a consequence, the net transport of the Kuroshio has a larger value in the meander-path years ( $38.6 \text{ Sv}$ ) than in the remaining years ( $28.9 \text{ Sv}$ ).

The path variations of the Kuroshio can strongly influence the surrounding water masses. One example of such influence was given in a recent study by Suga et al. (1989), who showed that less Subtropical Mode Water was detected during the large-meander years of the Kuroshio. To clarify other possible influences, we investigated fluctuations in the North Pacific Intermediate Water as well as the water-mass movement below the 1500-m depth. The NPIW, as we discussed briefly in section 3, is characterized by a salinity minimum south of the Kuroshio on a density surface of  $26.8\sigma_\theta$  (see Fig. 3). To quantify its fluctuations, we defined the NPIW core to be the cross-sectional area with  $S < 34.25 \text{ psu}$  (using other threshold values for the salinity core rendered essentially the same results). Figure 8 shows the time series of the size, the center latitude, and the average  $\sigma_\theta$  value of the NPIW core determined from the individual cruises. A high correlation in both amplitude and phase exists between the position changes of the NPIW core (Fig. 8b) and the Kuroshio axis (Fig. 6). Like the Subtropical Mode Water, the core size of the NPIW tends to decrease during the Kuroshio meander years (Fig. 8a). This

TABLE 2. Geostrophic transport of the Kuroshio, the Kuroshio Countercurrent, the North Equatorial Current, and the North Equatorial Countercurrent from individual cruises. Reference level is 1250 db for the Kuroshio and the KCC, and 1000 db for the NEC and NECC. Units are  $10^6 \text{ m}^3 \text{ s}^{-1}$  ( $\equiv \text{Sv}$ ).

|      |         | Kuroshio | KCC   | NEC   | NECC |
|------|---------|----------|-------|-------|------|
| 1967 | January | —        | —     | -59.4 | 52.2 |
| 1968 | January | —        | —     | -59.4 | 54.1 |
| 1969 | January | 48.4     | -20.5 | -55.5 | 36.3 |
| 1970 | January | 42.7     | -20.0 | -44.4 | 55.6 |
| 1971 | January | 48.2     | -15.9 | -51.1 | 31.6 |
| 1972 | January | 43.4     | -17.3 | -54.0 | 27.2 |
|      | July    | 46.7     | -17.1 | -81.6 | 75.8 |
| 1973 | January | 46.5     | -15.3 | -47.8 | 76.2 |
|      | July    | 55.1     | -21.7 | -57.8 | 46.4 |
| 1974 | January | 39.2     | -26.0 | -47.2 | 28.1 |
|      | July    | 42.3     | -24.5 | -66.8 | 47.8 |
| 1975 | January | 31.7     | -11.6 | -54.2 | 22.8 |
|      | July    | 37.5     | -10.6 | -33.5 | 30.0 |
| 1976 | January | 56.2     | -17.4 | -43.3 | 27.9 |
|      | July    | 43.7     | -7.9  | -66.7 | 71.4 |
| 1977 | January | 47.6     | -2.1  | -76.0 | 67.3 |
|      | July    | 42.4     | -0.5  | -70.5 | 67.3 |
| 1978 | January | 49.9     | -17.0 | -58.3 | 55.6 |
|      | July    | 65.2     | -22.4 | -43.4 | 41.2 |
| 1979 | January | 48.1     | -0.7  | -66.0 | 49.2 |
|      | July    | 46.7     | -2.3  | -67.9 | 72.5 |
| 1980 | January | 48.5     | -11.1 | -75.3 | 73.9 |
|      | July    | 53.0     | -22.1 | -77.1 | 77.8 |
| 1981 | January | 57.8     | -21.4 | -71.1 | 62.5 |
|      | July    | 80.3     | -41.5 | -62.1 | 65.6 |
| 1982 | January | 68.9     | -27.4 | -55.2 | 40.7 |
|      | July    | 51.1     | -10.7 | -73.3 | 67.0 |
| 1983 | January | 54.6     | -18.0 | -69.8 | 66.4 |
|      | July    | 65.2     | -18.5 | -61.7 | 33.6 |
| 1984 | January | 49.6     | -5.5  | -44.3 | 38.1 |
|      | July    | 63.6     | -32.1 | -80.2 | 24.0 |
| 1985 | January | 53.8     | -24.2 | -65.1 | 44.3 |
|      | July    | 58.9     | -34.1 | -68.3 | 54.5 |
| 1986 | January | 40.1     | -8.7  | -63.6 | 46.1 |
|      | July    | 66.5     | -35.9 | -82.5 | 73.4 |
| 1987 | January | 52.7     | -15.7 | -64.9 | —    |
|      | July    | 62.5     | -16.0 | -90.5 | —    |
| 1988 | January | 50.7     | -8.7  | -61.6 | 71.2 |
|      | July    | 65.7     | -31.1 | -57.8 | 30.6 |

tendency was particularly clear in the years 1976 to 1979 when the core was reduced to almost half the size observed in the straight-path years. In contrast to the vigorous changes in size and horizontal position associated with the Kuroshio meanders, Fig. 8c reveals that the NPIW core has remained rather consistently on the  $26.8\sigma_\theta$  surface throughout the past two decades. Combining the results in Fig. 8 suggests that when a Kuroshio meander develops, the NPIW, which is advected westward from the central North Pacific, is unable to detour southward around the meander on the  $26.8\sigma_\theta$  surface. The weakening of the Kuroshio's southern recirculation (the KCC) during the meander years is a possible reason for the observed large reduction in the NPIW size.

Water-mass movement below the main thermocline is more difficult to detect because there is no particular water mass, such as the NPIW, that can be used as a

“tracer.” However, the  $\theta$ - $S$  relations in Fig. 2 showed that between the density surfaces of  $27.65\sigma_\theta$  and  $27.75\sigma_\theta$  (which correspond roughly to the depths of 1500 m and 2500 m, see Fig. 3c), water masses changed monotonically from warm and saline in the south to cold and fresh in the north. Since the  $\theta$ - $S$  curves have this monotonic gradient, it is possible to detect water-mass movement by tracking a water mass with a particular  $\theta$ - $S$  relation. To do so, we tracked the water mass that has an average  $\theta$ - $S$  relation of the southernmost and northernmost water mass end points (bin 1 and 7 in Fig. 2). Figure 9 shows the time series of its position averaged in the 1500–2500-m layer. During the three meander-path periods of 1976–80, 1982–84, and 1987–88, Fig. 9 reveals a general tendency for this middepth water mass to shift northward. This shift may be a manifestation of a compensating flow that supplies the lower-layer water into the region between the meandering Kuroshio and the Japan coast. This region is often referred to as the “cold water mass region” and evidence of upwelling during the meander years of 1976–80 has been given by Nishida (1982) and Ishii et al. (1983).

Compared to the NPIW, the association of the mid-depth water-mass movement with the Kuroshio meander is less definite. There are position changes in Fig. 9 that seem to be unrelated to the occurrence of the Kuroshio meanders. Nevertheless, it is worth emphasizing that the influence of the Kuroshio path change may not only be confined to the upper layer in

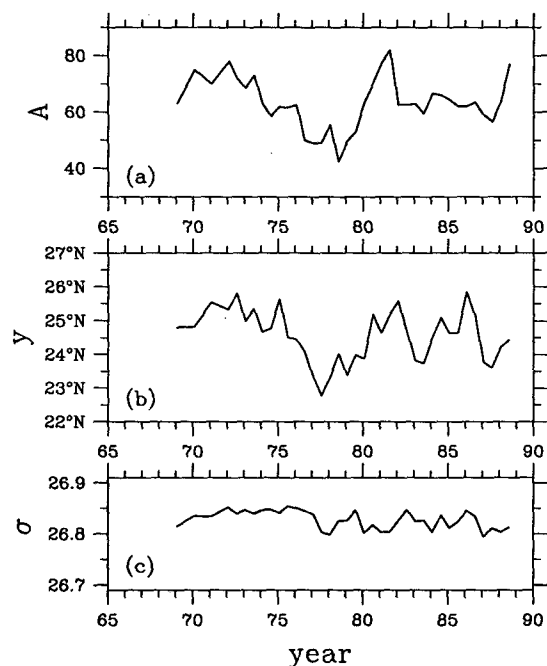


FIG. 8. Variations of the salinity minimum core ( $S < 34.25$  psu) of the North Pacific Intermediate Water: (a) the size (units are in meter  $\times$   $5^\circ$  latitude), (b) the center latitude, and (c) the average  $\sigma_\theta$  value in the core.

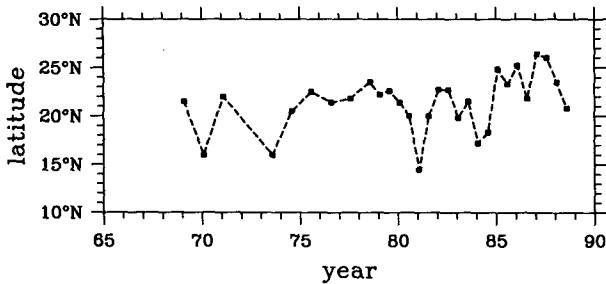


FIG. 9. Time series of the latitudinal position of the water mass that has an equal mixed ratio of the southernmost and northernmost origins in the 1500–2500-m layer (see text for details).

the thermocline, but may be further related to the interannual changes of the middepth water masses.

5. Low-latitude interannual variability

In the low latitude south of 20°N, the surface dynamic height anomalies in Fig. 5 exhibited a somewhat different variation pattern from the midlatitude region: the height anomaly field had a spatially coherent structure and was more periodic with an oscillation period of a few years. To extract this coherent structure from the smaller-scale fluctuations, we decomposed the height anomaly field between 2°N and 20°N into empirical orthogonal functions (EOFs). The coherent variation is essentially contained in the first EOF, which explains 60.1% of the total variance (Fig. 10; the variance explained by the second and higher modes drops sharply down to 16.1% and less). The spatial structure of the first EOF in Fig. 10a reveals that this spatially coherent signal is centered near 6°N, close to the boundary between the NEC and the NECC, and tapers off gradually northward and southward. Significant surface height drops are found in the years of 1969, 1972–73, 1976, 1980, 1982–83, and 1986–87, respectively (Fig. 10b). Except for the year 1980, all of these large-scale height drops concurred with the El Niño events in the eastern tropical Pacific. While there was only weak indication of an El Niño episode in the eastern tropical Pacific, zonal wind, surface salinity, and rainfall data in the western equatorial Pacific from the end of 1979 through 1980 all indicated typical patterns associated with the ENSO events (strong westerly wind burst, negative salinity anomaly, and excessive rainfall; see Donguy et al. 1982). The significant drop in the surface dynamic height anomaly shown in Fig. 10b further confirms such an ENSO episode in the western Pacific. In the following analysis, the year 1980 was consequently categorized under the “ENSO years.” Due to its weak amplitude, the year 1974 was not regarded as an ENSO year.

Figure 11 shows the surface dynamic height profiles averaged for the ENSO (dashed line) and the non-ENSO years (solid line). The difference between the two profiles is most prominent in the low-latitude region and is characterized, as we have noted in Fig. 10,

by a spatially coherent drop in the surface dynamic height during the ENSO years. The trough of the surface dynamic height, which forms the boundary between the NECC and the NEC, shifts from an average of 7.5°N during the non-ENSO years to 6.5°N during the ENSO years. This southward shift of the height trough in the ENSO years is further accompanied by a southward shift in the southern boundary of the NECC (from a mean position at 3°N to 2°N). The northern boundary of the NEC, on the other hand, shows an opposite movement: the surface dynamic height ridge moved from the mean position at 18°N in the non-ENSO years to 20.5°N in the ENSO years.

In the non-ENSO years, the height differences across the NECC and the NEC ( $\Delta D_{\text{ridge}} - \Delta D_{\text{trough}}$ ) are on average 1.5 and 4.5  $\text{m}^2 \text{s}^{-2}$ , respectively. These values increase to 2.7 and 6.3  $\text{m}^2 \text{s}^{-2}$  in the ENSO years, indicating that both the NEC and the NECC have a larger transport in the ENSO years than in the non-ENSO years. In calculating the transport values of the NEC and the NECC, we defined the NECC as an eastward-flowing surface current within the latitude bands of 2°–8°N. Determining the northern boundary of the NEC was relatively difficult because the region between 18°N and 25°N was commonly filled with weak currents flowing alternately east- and westward. In defining the transport of the NEC, we integrated all flows from the southern edge of the NECC north of 18°N when a boundary with a major eastward flow (i.e., the subtropical countercurrent) was encountered. Figure 12 shows the time series of the NECC and NEC transport calculated from the individual cruises. The mean transport values are 51.5 Sv for the NECC and –62.3 Sv for the NEC (Table 1). While the mean transport value of the NEC is close to that estimated from the

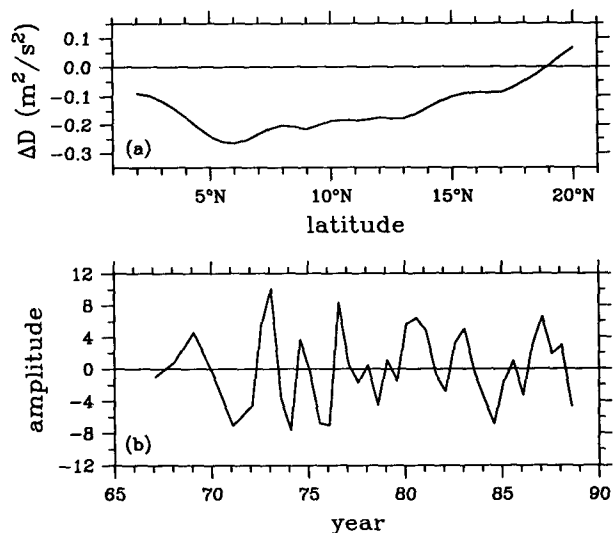


FIG. 10. The first EOF of the surface dynamic height anomaly field in the low-latitude region of 2°–20°N (Fig. 5). In the figure, (a) shows the spatial pattern and (b) shows its temporal amplitude. This EOF explains 60.1% of the total height variance.

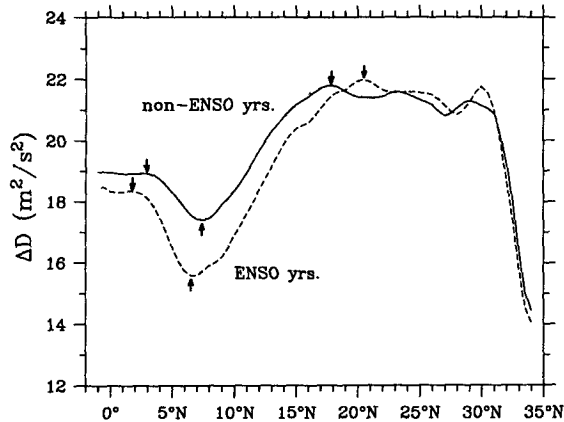


FIG. 11. Mean dynamic height profiles (0/1000 db) along the 137°E meridian averaged during the ENSO (dashed line) and non-ENSO (solid line) years. Arrows indicate the surface boundaries for the NEC and the NECC.

mean distributions of  $\theta$  and  $S$  ( $-59.4$  Sv), the mean transport value of the NECC is about 20% (10 Sv) larger than that estimated from Fig. 4 (41.7 Sv). This difference between estimations from the geographically fixed coordinate and the stream coordinate is essentially due to the larger meridional shifting of the NECC (compared to the current's width) than that of the NEC.

Averaging the transport values of the NECC and the NEC over the ENSO and non-ENSO years revealed that the amplitudes of the interannual change in the NECC and the NEC are 26.3 and 13.8 Sv, respectively (Table 1). In addition to these interannual variations associated with the ENSO events, annual signals also exist in the NECC and the NEC. On average, transports are larger in summer than in winter. The difference between the two seasons is 6.0 Sv for the NECC and 8.7 Sv for the NEC. The amplitude ratio of the annual signal to the interannual signal is thus 0.23 for the NECC and 0.63 for the NEC. In Fig. 12, the difference due to this different ratio is obvious: while the fluctuations in the NECC are dominated by the ENSO signals, this tendency is less clear in the time series of the NEC due to relatively small amplitude of the interannual signal and contamination from the annual variations.

Due to the abundance of near-surface expendable and mechanical bathythermograph (XBT and MBT) observations, many previous investigators have studied the low-frequency variability of the North Pacific using the water temperature data alone (e.g., Meyers 1979; White et al. 1982, 1985a; Kessler 1990). It is of interest to clarify how the fluctuations in the surface dynamic height, calculated here using both temperature and salinity data, are related to the fluctuations in the water temperature field. To do so, we calculated depths of the 12°C isotherm from the 39 cruises. In the low-latitude region, the 12°C isotherm appears near the bottom of the thermocline (Fig. 3a) and changes in its depth can be understood physically as changes of the

upper-layer thickness ( $h$ ). In the midlatitudes, the 12°C isotherm more or less exists in the upper portion of the thermocline. Figure 13 shows the anomaly field associated with the 12°C isotherm depth (as in Fig. 5, the anomalies are defined as the departures from the seasonal averages). Negative anomalies in Fig. 13 denote the shoaling of the isotherm and their appearance in low latitudes coincides with the drop of the surface dynamic height during the ENSO events.

The relationship between the anomaly field of  $\Delta D$  and that of the 12°C isotherm depth becomes clearer when the depth anomaly values are plotted against the  $\Delta D$  anomaly values. Figure 14 shows the result for all data points that fall within the region of 1°S–25°N. The correlation between the two anomaly fields is high, with a correlation coefficient of .82. The high correlation between the anomalies of isotherm depth and dynamic height was previously noted by Rebert et al. (1985) using XBT data and standard  $T$ - $S$  curves. Physically, it implies that the interannual variability found in the low latitudes occurs mainly in the upper layer above the thermocline and its underlying dynamics can be understood in the framework of a reduced gravity model. A least-squares fit of the slope in Fig. 14 reveals the value of the reduced gravity  $g' = 0.051 \text{ m s}^{-2}$ .

## 6. Discussion

### a. Geostrophic transport versus Sverdrup transport

In the last section, we found that the interannual fluctuations in the low latitudes along 137°E were

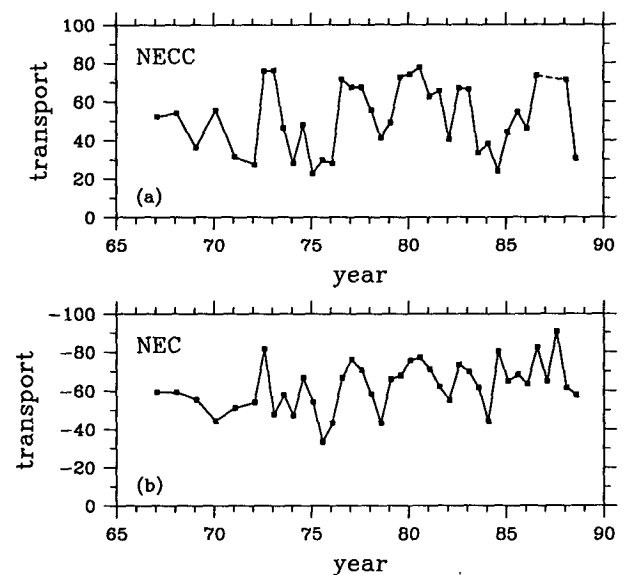


FIG. 12. Time series of the geostrophic transport of the North Equatorial Current and the North Equatorial Countercurrent (units: Sv). Notice that the hydrographic survey terminated at 3°N during summer and winter cruises in 1987 as well as the summer of 1988. We were only able to estimate the NECC's transport for the 1988 summer cruise when the equatorial Pacific was in the La Niña phase and the NECC shifted northward.

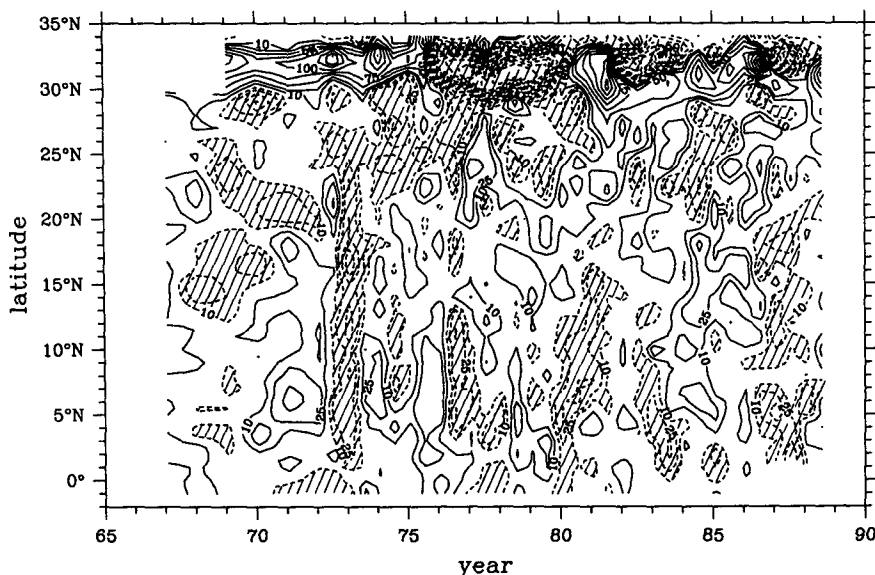


FIG. 13. Same as in Fig. 5 except for the upper-layer thickness anomalies (units are in meters). The upper-layer thickness is defined by the 12°C isotherm depth.

strongly related to the ENSO events that occur in the equatorial Pacific Ocean. In order to further clarify this connection, we investigated variations of the wind-stress curl field based on the FSU surface wind dataset (1965–89). Since the focus of the study was on the interannual variability, the wind-stress curl data were low-pass filtered to remove frequencies greater than once per year. Figure 15 shows the wind-stress curl fluctuations integrated over the tropical and subtropical North Pacific regions. Both the tropical and subtropical wind gyres had clear ENSO signals and intensified during the ENSO years (interpretation of the subtropical wind gyre requires some caution: since the FSU wind data are limited to south of 30°N, the dashed line in Fig. 15 shows the intensity of the subtropical wind gyre only in its southern portion). The basin-scale fluctuations in the wind field will undoubtedly affect the Sverdrup transport of the interior ocean. While the interior ocean response to the wind fluctuations is a time-dependent process, it is interesting to estimate how much the Sverdrup transport fluctuations can account for the observed transport fluctuations of the NEC and the NECC in the interannual frequency band. Effects due to time-dependent wave propagation will be considered later using a reduced gravity model.

By integrating the wind-stress curl data from the eastern boundary, we show in Fig. 16 the Sverdrup transport streamline fluctuations along the 137°E meridian. From this figure, we evaluated the Sverdrup transport for the NEC using the maximum difference in the streamline values and that for the NECC from the difference between the minimum streamline value and the streamline value at 2°N. The results are shown in Fig. 17 by solid lines. Superimposed on Fig. 17 by dashed lines are the geostrophic transport time series

from the hydrographic surveys (cf. Fig. 12). Notice that the mean geostrophic transport value of the NECC is larger than that from the Sverdrup balance (as was noted in section 3). For comparison, we used the geostrophic transport values of the NECC above the 12°C isotherm in Fig. 17a. A nearly constant offset (~15 Sv) exists between the time series shown in Fig. 12a and those defined above the 12°C isotherm. Reasons for this constant offset will be discussed in subsection 6c.

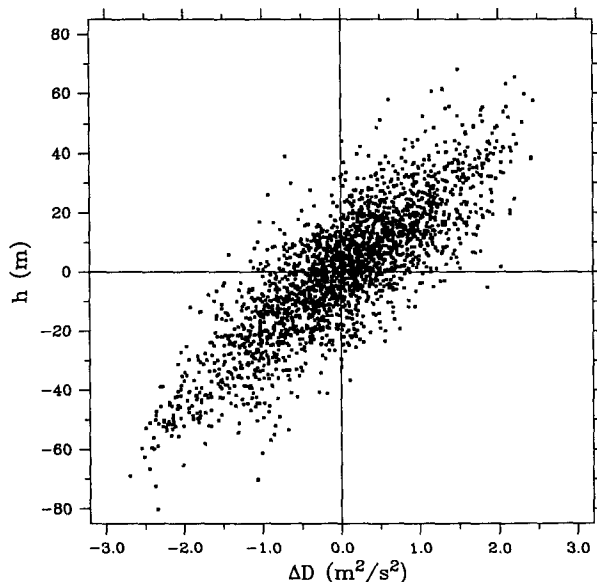


FIG. 14. Scatter diagram between anomaly values of the surface dynamic height ( $\Delta D$ , Fig. 5) and the upper-layer thickness ( $h$ , Fig. 13) in the region from 1°S to 25°N.

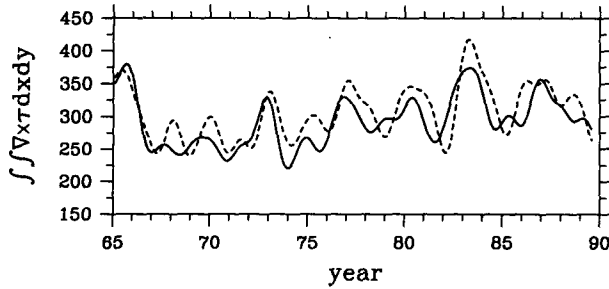


FIG. 15. Time series of the wind-stress curl over the tropical (solid line) and subtropical (dashed line) ocean gyres. The solid (dashed) line is calculated by integrating the positive (negative) wind-stress curl values in the region of  $0^{\circ}$ – $20^{\circ}$ N ( $10^{\circ}$ N– $30^{\circ}$ N) based on the low-pass-filtered FSU wind data. Units:  $4 \times 10^3 \text{ N m}^{-1}$ .

The correlation between the geostrophic and Sverdrup transports in Fig. 17 is generally good, especially during the ENSO events of 1972–73, 1976, 1980, and 1982–83. Phase delays between the transport peaks are in most cases shorter than the 6-month interval, the temporal resolution of the hydrographic surveys. The correspondence between the two time series is poor before 1971 and after 1984. The poor correspondence before 1971 may result from the fact that the hydrographic surveys then were only performed once per year in January. After 1984, the geostrophic transport fluctuations in the NEC are dominated by annual signals. Since the Sverdrup transport time series in Fig. 17 included no annual signals, a better comparison for the NEC is to use a time series of the geostrophic transport with the annual signals removed. In Fig. 18, we constructed this time series (dashed line) using the first EOF of the surface height anomaly field and compared it with the Sverdrup transport anomalies of the NEC.

In converting the  $\Delta D$  anomaly ( $\Delta D'$ , Fig. 10) to the transport anomaly ( $T'$ ), we used

$$T' = - \int_{6^{\circ}}^{20^{\circ}} \frac{H}{f} \frac{\partial \Delta D'}{\partial y} dy, \quad (1)$$

where  $H$  is the upper-layer thickness defined by the  $12^{\circ}\text{C}$  isotherm. In a reduced gravity model,  $T'$  gives the transport anomaly in the upper layer. The correlation between these two time series is remarkable. It is worth mentioning that the correlation in Fig. 18 improved not only because the two time series were consistent (included only interannual signals). More importantly, the transport fluctuations computed from the first EOF of the  $\Delta D'$  field reduced the effects of small-scale fluctuations. It is likely that the small-scale transport fluctuations are not directly related to the interannual fluctuations of the basin-scale wind-stress curl field.

#### b. Time-dependent responses

In the preceding discussion, we have assumed that the ocean interior response to the surface wind forcing in the interannual frequency band is steady. The good correlation between the fluctuations of the Sverdrup and geostrophic transports of both the NECC and the NEC may appear as a surprise because in the higher-latitude NEC region, one would expect the oceanic response to lag behind that in the lower-latitude NECC region due to the slower propagation of the baroclinic Rossby waves. In fact, a simple calculation, assuming periodic changes in the wind-stress curl magnitude and a constant  $c = (g'H)^{1/2}$  value for the first baroclinic mode, reveals that the response in the NEC region

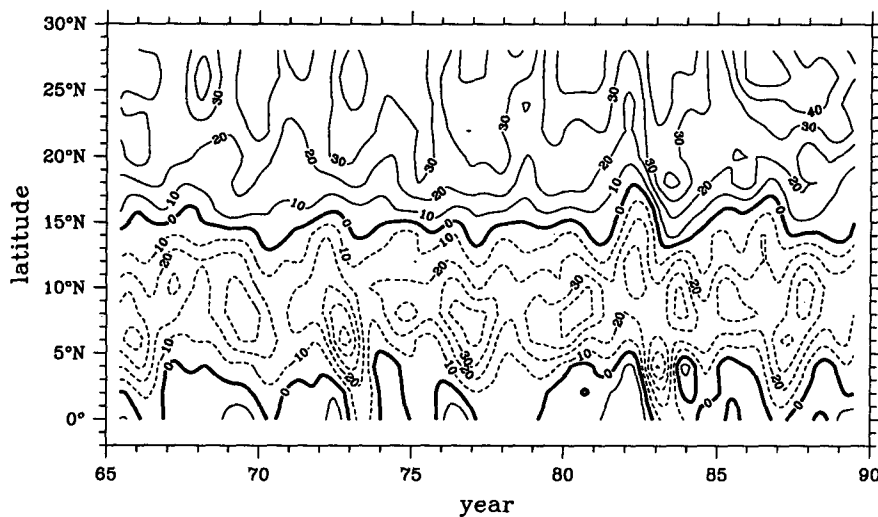


FIG. 16. Fluctuations of the Sverdrup transport streamlines along the  $137^{\circ}\text{E}$  meridian estimated from the low-pass-filtered FSU wind data. Units are in Sverdrups.

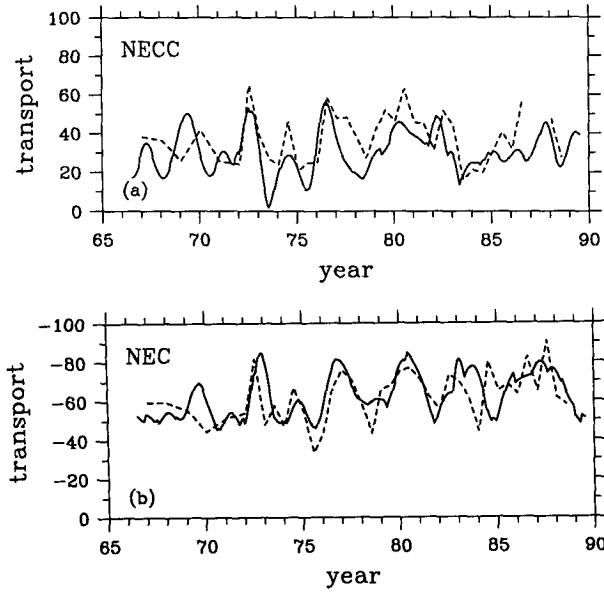


FIG. 17. Comparisons between time series of the Sverdrup transport (solid line) and the geostrophic transport (dashed line) for (a) the NECC and (b) the NEC. Notice that the geostrophic transport of the NECC in (a) is the eastward flow above the 12°C isotherm.

would be weak and lag considerably behind that in the NECC region (Fig. 19a).

To further clarify this point, we considered the time-dependent oceanic response of the western North Pacific to the basin-scale wind fluctuations. In a reduced gravity model (see section 5 for its validity), large-scale, low-frequency motions in the off-equatorial, low-latitude ocean are governed by

$$\frac{\partial h}{\partial t} - \left(\frac{\beta c^2}{f^2}\right) \frac{\partial h}{\partial x} = -\frac{1}{\rho} \text{curl} \left(\frac{\boldsymbol{\tau}}{f}\right) \quad (2)$$

(e.g., Meyers 1979), where  $h(x, y, t)$  is the height deviation from the mean upper-layer thickness  $H(y)$ ,  $\boldsymbol{\tau}$  is the vector of the wind-stress anomaly, and  $c = (g'H)^{1/2}$  is the speed of the internal gravity wave.

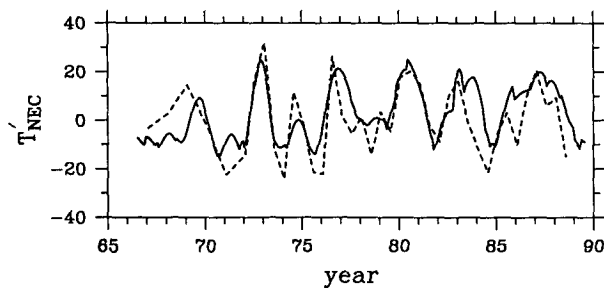


FIG. 18. Comparison between the transport fluctuations in the NEC from the Sverdrup balance (solid line) and from the transport calculation based on the first EOF of the surface dynamic height anomaly [dashed line, see Eq. (1)].

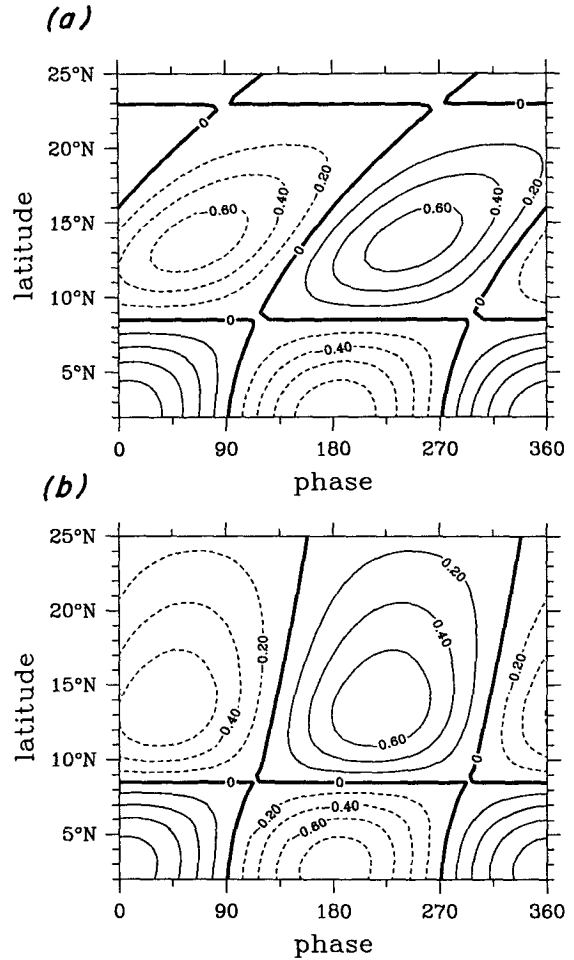


FIG. 19. Patterns of the zonal velocity anomaly  $u$  along 137°E induced by basinwide wind-stress curl fluctuations in a reduced gravity model [see Eq. (4), units are arbitrary]. In (a), the mean upper-layer thickness is constant ( $H = 250$  m) and the wind forcing is zonally independent. In (b), the upper-layer thickness is determined from the mean 12°C isotherm depth and the wind forcing is centered at the date line with a longitudinal decay scale of  $\sigma^{-1} = 2500$  km. Other common parameters for (a) and (b) are  $\omega = 5.7 \times 10^{-8} \text{ s}^{-1}$ ,  $x = -11,000$  km,  $g' = 0.051 \text{ m s}^{-2}$ ,  $L = 13^\circ$  latitude for the tropical gyre ( $2^\circ$ – $15^\circ$ N), and  $L = 27^\circ$  latitude for the subtropical gyre ( $15^\circ$ – $42^\circ$ N), respectively.

In the presence of mean zonal flows,  $c$  in Eq. (2) is a function of  $y$ . Since the intensity of the tropical and subtropical gyres fluctuates quasi-periodically (Fig. 15), we expressed the wind-stress curl fluctuation as follows:

$$\text{curl} \boldsymbol{\tau} \sim \exp(-\sigma|x - x_o|) \cos(\omega t) \sin\left(\frac{\pi}{L} y\right). \quad (3)$$

In (3), the fluctuating wind-stress curl field has a center at  $x = x_o$  with a decay scale of  $\sigma^{-1}$  and a wave frequency of  $\omega$ . Meridionally, the fluctuation is assumed to have the same double-gyre structure as the mean wind-stress curl field and  $L$  is the gyre's meridional scale. Assuming  $h = 0$  at the eastern boundary ( $x = 0$ ), the oceanic

response west of  $x_0$  to such a wind-stress curl fluctuation is simply

$$h \sim \frac{\lambda}{\rho f w} \exp(i\omega t) \times \sin\left(\frac{\pi}{L} y\right) \left[ \frac{1}{\sigma + i\lambda} (e^{\sigma x_0 + i\lambda x} - e^{i\lambda(x-x_0)}) + \frac{1}{\sigma - i\lambda} (e^{\sigma(x-x_0)} - e^{i\lambda(x-x_0)}) \right], \quad (4)$$

where  $\lambda = \omega f^2 / (\beta c^2)$ .

It is instructive to consider the case when  $c$  is constant and  $\sigma \rightarrow 0$  (no mean zonal flow and uniform wind-stress curl fluctuation in  $x$ ). In this case, the geostrophic zonal velocity  $u$  along a meridian is given by

$$u \sim -\frac{1}{f^2} \cos\left(\frac{\lambda}{2} x + \omega t\right) \sin\left(\frac{\lambda}{2} x\right) \cos\left(\frac{\pi}{L} y\right). \quad (5)$$

Figure 19a shows the  $u$  response along the 137°E meridian based on parameters appropriate for the North Pacific. In the NECC region, an increase of the eastward zonal velocity occurs almost simultaneously with the forcing amplitude. For the wind forcing fluctuating with a period of about 3.5 years, the temporal lag in the maximum NECC transport (the integral of the zonal velocity between 2°N and 8.5°N) is  $O(1)$  month. In the NEC region, the zonal velocity pattern depends strongly on the latitude. From Eq. (5), the temporal lag of the maximum  $u$  response is

$$t = -\frac{\lambda}{2\omega} x = -\frac{f^2 x}{2\beta c^2}. \quad (6)$$

Physically, the temporal lag is determined by the distance from the center location of the wind forcing to the observational meridian ( $x/2$  in this case) divided by the phase speed of the long baroclinic Rossby wave ( $\beta c^2 / f^2$ ). With the increase in latitude, the  $u$  response delays due to the decrease in the phase speed of the long baroclinic Rossby wave. The strong latitudinal dependence of the  $u$  response in Fig. 19a weakens the transport fluctuations (i.e., the  $y$  integral of  $u$ ) of the NEC.

In the observed wind-stress curl field over the North Pacific, the interannual fluctuation associated with the ENSO events north of the equator has its center near the date line and has a zonal decay scale of a few thousand kilometers (Kessler 1990, his EOF result of Fig. 18). This indicates that the center of the wind forcing is located closer to the 137°E meridian than that of a zonally uniform forcing. Moreover, the mean upper-layer thickness  $H(y)$  in the NEC region increases northward, consequently increasing the internal gravity wave speed  $c$ . As indicated in Eq. (6), both of these factors tend to decrease the temporal delay toward the midlatitudes due to the increasing  $f$  value. Figure 19b shows the  $u$  response along 137°E when these two factors were taken into account. The latitudinal depen-

dency of the phase compared to Fig. 19a is largely suppressed in the NEC region, suggesting that we can expect significant transport variations in the NEC. Figure 19b also suggests that the maximum transport of the NEC would lag about 45° in phase (or about 5.3 months) behind the wind-stress curl maximum. Unfortunately, the biannual observations along 137°E are too coarse in time to test this temporal lag.

Based on this simple model calculation, we conclude that the high correlation between the interannual fluctuations in the low-latitude western North Pacific and those in the wind-stress curl field is possibly due to 1) the center of the wind forcing field being located close to the western North Pacific (near the date line) and 2) the weaker decrease of the long baroclinic Rossby wave speed with increasing latitude due to the deepening of the thermocline associated with the presence of the NEC.

### c. NECC and NSCC

The good agreement between the Sverdrup and geostrophic transport changes in the NECC contrasts with the large difference in the mean values of the two quantities: the mean NECC transport between 2° and 8°N is 42 Sv, nearly 14 Sv greater than expected from the mean Sverdrup transport. This discrepancy has been noted by others (Spillane and Niiler 1975; Meyers 1980) and it has been argued that the Sverdrup vorticity balance is not appropriate for the narrow NECC. In the present study, we found that the NECC's fluctuations above the 12°C isotherm agree well with the Sverdrup transport fluctuations and that there is nearly a constant offset between the total eastward transport and the eastward transport above the 12°C isotherm (cf. Figs. 12a and 17a). These two facts suggest that this discrepancy can be due to the definition of the NECC. Several previous studies separated the eastward flow in the 2°–8°N region into the NECC and the Northern Subsurface Countercurrent (NSCC). In particular, Tsuchiya (1975) and Hayes et al. (1983) noticed that the NSCC in the eastern equatorial Pacific had a high degree of stability and was not simply a deep expression of the NECC. Their findings also apply well to the western equatorial Pacific along 137°E.

If the NECC above the 12°C isotherm, as we found previously, is driven by the tropical wind gyre, what then causes the NSCC, the eastward flow below the thermocline? Using a continuously stratified model, McPhaden (1984) proposed that the NSCC existing at the edge of a diffusive equatorial-vorticity boundary layer can be driven by diffusion of the cyclonic vorticity of the equatorial undercurrent. However, Kitamura and Sugimoto (1987) found that the strength of the NSCC in their numerical model, which included nonlinearity, dissipation, and diffusion, was an order of magnitude weaker than observed. A second possible driving force for the NSCC is the thermohaline circulation, an internal mode that cancels out in a vertical

average. Observations of low silica water at 2000-m depth spreading northward along the western boundary near 137°E (Talley and Joyce 1992) support a southern source and a deep northwestward flow along the western boundary of the equatorial Pacific. If this flow is part of the thermohaline circulation, there must be an opposite, compensating flow in the upper ocean that could contribute to the NSCC. Near the western boundary of the equatorial Pacific where the EUC is not yet formed, we speculate the thermohaline circulation driven by inflows from the South Pacific to be important for the NSCC.

#### d. Decadal trend in the subtropical gyre

In Fig. 7, both the Kuroshio transport and the net transport of the Kuroshio displayed a gradual increase in the decadal time scale. A similar gradual increase, with an increase rate of about 5 Sv/decade, also appeared in the transport time series for the NEC in the past two decades (see Fig. 12b). This trend is likely related to the steady increase in the magnitude of the subtropical wind gyre over the North Pacific from the late 1960s (see Fig. 15).

### 7. Conclusions

Using the hydrographic data collected along the 137° meridian by the Japan Meteorological Agency and the surface wind data compiled by Florida State University, we investigated the interannual variability in the mid- and low-latitude western North Pacific from 1967 to 1988. In the midlatitude region north of 22°N, we found that fluctuations in the dynamic height field were essentially related to the interannual changes of the Kuroshio, namely, its bimodal path variation. From the 22-year time series of hydrographic data covering the three meander events of 1976–80, 1982–84, and 1987–88, we showed that whereas the eastward transport of the Kuroshio per se exhibited no significant dependency on the path variations, there was on average a 30% increase in the net transport of the Kuroshio system (the Kuroshio plus its recirculations) during the meander years. This increase, from an average of 28.9 Sv in the straight-path years to 38.6 Sv in the meander-path years, was largely manifested by the weakening of the Kuroshio Countercurrent.

Since the net transport of the Kuroshio is likely determined by the Kuroshio transport in the upstream region, the result of the present study supports the analyses by Kawabe (1980) and Saiki (1982) that the Kuroshio transport in the East China Sea and at the Tokara Strait is larger in the meander-path years than in the straight-path years. Due to large variations in the KCC, the Kuroshio transport value south of Japan is not by itself the appropriate quantity for determining the relation between the Kuroshio transport and its path variations.

The Kuroshio path variations strongly influenced the North Pacific Intermediate Water (the salinity

minimum at densities of 26.5 to 27.0 $\sigma_\theta$ ) and the water-mass movement below the thermocline. During the Kuroshio meander years, the salinity minimum core of the NPIW ( $S < 34.25$  psu) not only shifted southward with an amplitude similar to the horizontal excursions of the Kuroshio meanders (2–3 degrees of latitude), but there was also a significant decrease in the size of the NPIW. Coinciding with the weakening of the Kuroshio Countercurrent, this size reduction suggested that when a Kuroshio meander develops, a significant portion of the NPIW is prevented from subducting farther westward due to the blocking of the meander. In the middepth layer between the 1500- and 2500-m depth, analysis of the  $\theta$ – $S$  relation revealed that there was a water-mass movement negatively correlated to the upper-layer Kuroshio path variations. In the meander-path years, the water mass tended to move northward, suggesting the existence of a compensating flow at the middepth layer for the cold-core eddy that develops between the meandering Kuroshio and the Japan coast.

In the low-latitude region along 137°E, we found that the surface height anomalies were highly correlated with the anomalies of the upper-layer thickness (defined by the depth of the 12°C isotherm). Large-scale surface height fluctuations were centered at the boundary between the North Equatorial Current and the North Equatorial Countercurrent (around 6°N). Except for 1980, large surface height drops were concurrent with the ENSO signals in the eastern equatorial Pacific. In the ENSO years, both the NEC and the NECC had larger transports (–70.8 and 68.6 Sv on average) than in the non-ENSO years (–57.0 and 42.3 Sv on average). The in-phase fluctuations of the NEC and the NECC found in the present study are opposite to those found by White and Hasunuma (1980), who showed that the fluctuations in these two equatorial currents in the western North Pacific were out of phase. The present result, however, agrees with the study for the central North Pacific by Wyrski (1979) based on sea level data. The discrepancy between the present study and that of White and Hasunuma for the western North Pacific may be caused by the coarse resolution White and Hasunuma used in their analysis.

The integrated wind-stress curl over both the tropical and subtropical gyres (up to 30°N) of the North Pacific increases during the ENSO years. In the NECC region of 2°–8°N, we found that the Sverdrup transport fluctuations calculated from the low-pass-filtered FSU wind data agreed well in both amplitude and phase with the fluctuations of the upper-layer eastward geostrophic transport of the NECC (above the 12°C isotherm). Below the 12°C isotherm, the eastward geostrophic flow had a nearly constant transport of about 15 Sv. Unlike the surface NECC, which is driven by winds, we speculated that the thermohaline circulation near the western boundary of the equatorial Pacific causes this subsurface eastward flow. High correlation was also obtained between the geostrophic and Sver-

drup transport fluctuations in the NEC. Since the propagating speed of the long baroclinic Rossby wave decreases rapidly with increasing latitude, this high correlation appeared somewhat unexpectedly. Using a reduced gravity model, we showed that the strong latitude dependence of the long baroclinic Rossby wave in the NEC region was largely attenuated by the thermocline tilt associated with mean westward flow (the NEC).

*Acknowledgments.* The hydrographic data were provided by the Japan Oceanographic Data Center and the National Oceanographic Data Center to the WOCE Hydrographic Programme Office of Woods Hole Oceanographic Institution. The surface wind data were provided by Florida State University. This study benefited from many helpful discussions with Bill Kessler, John Toole, and Susan Wijffels. Criticism of an earlier version by Harry Bryden, Kathie Kelly, Bruce Warren, and two anonymous reviewers helped to improve the text. The WOCE Hydrographic Programme Office at WHOI is supported by NSF Grant OCE-8907815. We wish to acknowledge the support of WHOI for B. Qiu and NSF Grant OCE-899908 for T. M. Joyce.

## REFERENCES

- Akitomo, K., T. Awaji, and N. Imasato, 1991: Kuroshio path variation south of Japan. 1. Barotropic inflow-outflow model. *J. Geophys. Res.*, **96**, 2549–2560.
- Andow, T., 1987: Year-to-year variation of oceanographic sub-surface section along the meridian of 137°E. *Oceanogr. Mag.*, **37**, 47–73.
- Armi, L., and N. A. Bray, 1982: A standard analytic curve of potential temperature versus salinity for the western North Atlantic. *J. Phys. Oceanogr.*, **12**, 384–387.
- Chao, S.-Y., 1984: Bimodality of the Kuroshio. *J. Phys. Oceanogr.*, **14**, 92–103.
- , and J. P. McCreary, 1982: A numerical study of the Kuroshio south of Japan. *J. Phys. Oceanogr.*, **12**, 679–693.
- Delcroix, T., G. Eldin, and C. Henin, 1987: Upper ocean water masses and transport in the western tropical Pacific (165°E). *J. Phys. Oceanogr.*, **17**, 2248–2262.
- Donguy, J. R., C. Henin, A. Morliere, J. P. Rebert, and G. Meyers, 1982: Appearances in the western Pacific of phenomena induced by El Niño in 1979–80. *Trop. Ocean-Atmos. Newslett.*, **10**, 1–2.
- Goldenberg, S. R., and J. J. O'Brien, 1981: Time and space variability of tropical Pacific wind stress. *Mon. Wea. Rev.*, **109**, 1190–1207.
- Hanawa, K., 1987: Interannual variations in the winter-time outcrop area of Subtropical Mode Water in the western North Pacific Ocean. *Atmos.-Ocean*, **25**, 258–274.
- Hayes, S. P., J. M. Toole, and L. J. Mangum, 1983: Water mass and transport variability at 110°W in the equatorial Pacific. *J. Phys. Oceanogr.*, **13**, 153–168.
- Ishii, H., 1982: Variation of the Kuroshio cold eddy.—Large meander of the Kuroshio in 1975–1980 (II). *Rep. Hydrogr. Res.*, **17**, 229–239.
- , Y. Sekine, and Y. Toba, 1983: Hydrographic structure of the Kuroshio large meander—cold water mass region down to the deeper layers of the ocean. *J. Oceanogr. Soc. Japan*, **39**, 240–250.
- Kawabe, M., 1980: Sea level variations along the south coast of Japan and the large meander in the Kuroshio. *J. Oceanogr. Soc. Japan*, **36**, 97–104.
- , 1985: Sea level variations at the Izu Islands and typical stable paths of the Kuroshio. *J. Oceanogr. Soc. Japan*, **41**, 307–326.
- Kawai, H., 1969: Statistical estimation of isotherms indicative of the Kuroshio axis. *Deep-Sea Res.*, **16**, 109–115.
- Kessler, W. S., 1990: Observations of long Rossby waves in the northern tropical Pacific. *J. Geophys. Res.*, **95**, 5183–5217.
- , and B. A. Taft, 1987: Dynamic height and zonal geostrophic transports in the central tropical Pacific during 1979–84. *J. Phys. Oceanogr.*, **17**, 97–122.
- Kitamura, Y., and N. Suginoara, 1987: Effect of vertical viscosity and diffusivity on tropical ocean circulation—Subsurface eastward flow. *J. Oceanogr. Soc. Japan*, **43**, 1–20.
- Levitus, S., 1982: *Climatological Atlas of the World Ocean*, NOAA Prof. Paper No. 13, U.S. Govt. Printing Office, Washington, D.C., 173 pp.
- Lukas, R., and E. Firing, 1984: The geostrophic balance of the Pacific Equatorial Undercurrent. *Deep-Sea Res.*, **31**, 61–66.
- Masuda, A., 1982: An interpretation of the bimodal character of the stable Kuroshio path. *Deep-Sea Res.*, **29**, 471–484.
- Masuzawa, J., 1969: Subtropical mode water. *Deep-Sea Res.*, **16**, 463–472.
- , 1972: Water characteristics of the North Pacific central region. *Kuroshio: Its Physical Aspects*. H. Stommel and K. Yoshida, Eds., University of Tokyo Press, 95–127.
- , and K. Nagasaka, 1975: The 137°E oceanographic section. *J. Mar. Res.*, **33**, 109–116.
- McPhaden, M. J., 1984: On the dynamics of Equatorial Subsurface Countercurrents. *J. Phys. Oceanogr.*, **14**, 1216–1225.
- Meyers, G., 1979: On the annual Rossby wave in the tropical North Pacific. *J. Phys. Oceanogr.*, **9**, 663–674.
- , 1980: Do Sverdrup transports account for the Pacific North Equatorial Countercurrent? *J. Geophys. Res.*, **85**, 1073–1075.
- , 1982: Interannual variation in the sea level near Truk Island. *J. Phys. Oceanogr.*, **12**, 1161–1168.
- Nishida, H., 1982: Description of the Kuroshio meander in 1975–1980—Large meander of the Kuroshio in 1975–1980 (I). *Rep. Hydrogr. Res.*, **17**, 181–207.
- Nitani, H., 1972: Beginning of the Kuroshio. *Kuroshio: Its Physical Aspects*. H. Stommel and K. Yoshida, Eds., University of Tokyo Press, 129–163.
- , 1975: Variation of the Kuroshio south of Japan. *J. Oceanogr. Soc. Japan*, **31**, 154–173.
- Rebert, J. P., J. R. Donguy, G. Eldin, and K. Wyrki, 1985: Relations between sea level, thermocline depth, heat content, and dynamic height in the tropical Pacific Ocean. *J. Geophys. Res.*, **90**, 11 719–11 725.
- Reid, J. L., 1965: Intermediate water of the Pacific Ocean. *Johns Hopkins Oceanogr. Stud.*, No. 2, 58 pp.
- Robinson, M. K., 1976: Atlas of North Pacific Ocean monthly mean temperatures and mean salinities of the surface layer. Naval Oceanographic Office reference publication 2, 194 pp.
- Saiki, M., 1982: Relation between the geostrophic flux of the Kuroshio in the East China Sea and its large-meander in the south of Japan. *Oceanogr. Mag.*, **32**, 11–18.
- Sekine, Y., and Y. Toba, 1981: Velocity variation of the Kuroshio during the small meander formation south of Kyushu. *J. Oceanogr. Soc. Japan*, **37**, 87–93.
- Shoji, D., 1972: Time variation of the Kuroshio south of Japan. *Kuroshio: Its Physical Aspects*. H. Stommel and K. Yoshida, Eds., University of Tokyo Press, 217–234.
- Spillane, M., and P. P. Niiler, 1975: On the theory of strong, mid-latitude wind-driven circulation, I: The North Pacific Countercurrent as a quasi-geostrophic jet. *Geophys. Fluid Dyn.*, **7**, 43–66.
- Suga, T., K. Hanawa, and Y. Toba, 1989: Subtropical Mode Water in the 137°E section. *J. Phys. Oceanogr.*, **19**, 1605–1618.
- Taft, B. A., 1972: Characteristics of the flow of the Kuroshio south of Japan. *Kuroshio: Its Physical Aspects*. H. Stommel and K. Yoshida, Eds., University of Tokyo Press, 165–216.
- Talley, L. D., 1990: An Okhotsk Sea water anomaly: Implications for ventilation in the North Pacific. *Deep-Sea Res.*, **38**(Suppl), 171–190.
- , and T. M. Joyce, 1992: The double silica maximum in the North Pacific. *J. Geophys. Res.*, **97**, 5645–5480.

- Toole, J. M., E. Zou, and R. C. Millard, 1988: On the circulation of the upper waters in the western equatorial Pacific Ocean. *Deep-Sea Res.*, **35**, 1451–1482.
- Tsuchiya, M., 1975: Subsurface countercurrents in the Pacific Ocean. *J. Mar. Res.*, **33**(Suppl.), 145–175.
- , R. Lukas, R. A. Fine, E. Firing, and E. Lindstrom, 1989: Source waters of the Pacific Equatorial Undercurrent. *Progress in Oceanography*, Vol. 23, Pergamon, 101–147.
- White, W. B., 1975: Secular variability in the large-scale baroclinic transport of the North Pacific from 1950–1970. *J. Mar. Res.*, **33**, 144–155.
- , 1977: Secular variability in the baroclinic structure of the interior North Pacific from 1950–1970. *J. Mar. Res.*, **35**, 587–607.
- , and J. P. McCreary, 1976: On the formation of the Kuroshio meander and its relationship to the large-scale ocean circulation. *Deep-Sea Res.*, **23**, 33–47.
- , and K. Hasunuma, 1980: Interannual variability in the baroclinic gyre structure of the western North Pacific from 1954–1974. *J. Mar. Res.*, **38**, 651–672.
- , G. Meyers, and K. Hasunuma, 1982: Space/time statistics of short-term climatic variability in the western North Pacific. *J. Geophys. Res.*, **87**, 1979–1989.
- , —, J. R. Donguy, and S. E. Pazan, 1985a: Short-term climatic variability in the thermal structure of the Pacific Ocean during 1979–82. *J. Phys. Oceanogr.*, **15**, 917–935.
- , S. E. Pazan, and B. Li, 1985b: Processes of short-term climatic variability in the baroclinic structure of the interior western tropical North Pacific. *J. Phys. Oceanogr.*, **15**, 386–402.
- Wyrki, K., 1974: Equatorial currents in the Pacific 1950–1970 and their relation to the winds. *J. Phys. Oceanogr.*, **4**, 372–380.
- , 1975: El Niño—The dynamic response of the equatorial Pacific Ocean to atmospheric forcing. *J. Phys. Oceanogr.*, **5**, 572–584.
- , 1979: Sea level variations: Monitoring the breath of the Pacific. *Eos*, **60**, 25–27.
- , 1982: Eddies in the Pacific North Equatorial Current. *J. Phys. Oceanogr.*, **12**, 746–749.
- , and G. Meyers, 1976: The trade wind field over the Pacific Ocean. *J. Appl. Meteor.*, **15**, 698–704.
- , and B. Kilonsky, 1984: Mean water and current structure during the Hawaii-to-Tahiti Shuttle Experiment. *J. Phys. Oceanogr.*, **14**, 242–254.
- Yasuda, I., J.-H. Yoon, and N. Suginozono, 1985: Dynamics of the Kuroshio large meander-Barotropic model. *J. Oceanogr. Soc. Japan*, **41**, 259–273.
- Yoon, J.-H., and I. Yasuda, 1987: Dynamics of the Kuroshio large meander: Two-layer model. *J. Phys. Oceanogr.*, **17**, 66–81.
- Yoshida, K., and T. Kidokoro, 1967: A subtropical counter-current in the North Pacific—An eastward flow near the subtropical convergence. *J. Oceanogr. Soc. Japan*, **23**, 88–91.